Proceedings of the 2018 Design of Medical Devices Conference
DMD2018
April 9-12, 2018, Minneapolis, MN, USA
DMD2018-6862

Real-Time, Non-Contact Position Tracking of Medical Devices and Surgical Tools through the Analysis of Magnetic Field Vectors

Mohammad Odeh
Institute for Simulation and Training, University of Central Florida
Orlando, Florida, USA

Edward Daniel Nichols
Institute for Simulation and Training, University of Central Florida
Orlando, Florida, USA

Fluvio L Lobo Fenoglietto
Institute for Simulation and Training, University of Central Florida
Orlando, Florida, USA

Jack Stubbs
Institute for Simulation and Training, University of Central Florida
Orlando, Florida, USA

BACKGROUND

The adoption of robotically assisted surgeries is increasing at a dramatic rate. The *Da Vinci* "was used in 80% of radical prostatectomies performed in the U.S. for 2008, just nine years after the system went on the market" [8]. The *Da Vinci* is but one of the systems driving the development of more versatile, more cost-effective and more autonomous systems. Robotic systems require real-time, accurate position information of the anatomy and surgical instruments to allow the surgical team to perform critical tasks. For example, Renishaw's *neuromate* and Accuray's *CyberKnife* both require the precise location of fiducial markers [9]. Others, like Cambridge Medical Robotics' Versius and Medrobotics' *Flex* operators rely upon active imaging or access to direct line of sight [10].

As robotic systems continue to technically advance across a broad scope, the inherent technical requirement for spatial awareness data will only increase. Machine-learning algorithms driving the interconnected array of robotic surgical assistants envisioned by Verb Surgical need data for processing [11]; surgeons performing teleoperations will benefit from the availability of high-quality, real-time, auxiliary sensor information that enables extension of their dexterity and spatial awareness. Additionally, as these technologies proliferate, providers will require easily deployed, cost-effective user input systems for simulation programs designed to train aspiring and established healthcare professionals on using state-of-the-art medical tools.

To help advance this field and to fulfill an imperative to provide simulation inputs for our own training applications, The PD3D lab at the Institute for Simulation and Training has constructed a robust, scalable, highly-customizable, and non-intrusive system for dynamically tracking point objects in a volumetric space. We developed a system to track permanent magnets. Given that human tissues are permeable to magnetic flux, magnets can be well-characterized, and there exists a wide variety of open-sourced hardware, our system locates and tracks the motion of the any magnet, in a volumetric space within the range of our array. Ultimately, this extremely low-cost proof-of-concept prototype serves as a foundation for exploring this approach in the medical industry.

METHODS

Analytical Foundation

Magnetic fields are characterized by fundamental principles. Given a classic magnetic dipole centered at the origin, its magnetic induction can be expressed as:

$$\vec{\mathbf{B}} = \frac{\mu_0}{4\pi} * \frac{3\hat{\mathbf{r}}(\vec{\boldsymbol{\mu}} \bullet \hat{\mathbf{r}}) - \vec{\boldsymbol{\mu}}}{\mathrm{r}^3} \quad (1)$$

The relationship is dependent on the orientation and strength of its magnetic moment vector, given by $\vec{\boldsymbol{\mu}}$, as well as the location of the arbitrary point of interest with respect to the center of the magnet, represented by vector $\vec{\mathbf{r}}$. Equation (1) can be modified to express the strength of the magnetic field $\vec{\mathbf{H}}$, which is what an observing magnetometer normal to the level surface of the magnetic field perceives; which may further be broken into a more convenient polar component form, given the intrinsic rotational symmetry of isofield lines about $\vec{\boldsymbol{\mu}}$. Based on the work of Chen *et al.* [5], expressing the location of the center of a magnet with respect to the magnetic field vectors observed by three sensors in predefined relative positions fully satisfies a system of equations when the magnet is in a fixed North pole orientation along the system's internally defined x-axis:

$$\left\|\vec{\mathbf{H}_i}\right\| = \sqrt{\frac{\mathrm{K}(3\cos^2\theta_i + 1)}{{r_i}^6}} \quad (2)$$

$$\|\vec{\mathbf{r}_i}\| = \sqrt{(\mathrm{x} + \Delta x_i)^2 + (\mathrm{y} + \Delta y_i)^2 + (\mathrm{z} + z_i)^2} \quad (3)$$

$$\cos\theta_i = \frac{z}{r_i} \quad (4)$$

Each sensor in the array is represented by i, $\|\vec{\mathbf{r}_i}\| = r_i$ is the distance to the center of the magnet for the sensor, Δ_i is the relative offset from a designated origin with respect to the sensor,

θ_i represents the angle made by the north pole of the magnet and the radial component of $\vec{\mathbf{H}}$, and K represents a constant that encompasses the magnitude of the dipole moment, magnetic permeability of free space μ_0, and the relative permeability of the magnet's own material.

Certain minimum conditions for a solution to converge numerically must be met:

1. An origin must be defined with respect to the relative fixed positions and orientations of the sensors.
2. The constant value of the magnetic field strength coefficient K of an arbitrary magnet has been closely approximated or is otherwise known.
3. A constant magnetic field source of perceivable threshold exists within the optimal range of at least three sensors in the sensor array.

In addition, to refine accuracy, certain physical restrictions facilitate these conditions:

1. Ambient magnetic fields must be mitigated; or their noise must be otherwise overcome.
2. The magnet's form factor is minimized to yield closer adherence to presupposed principles.

To begin achieving these conditions, we designated the sensor in the bottom left corner of our sensor array (Figure 1) to be the origin. All sensors' axes in the array are aligned with each other.

Magnet Selection

Permanent magnets were chosen to enable a simple but versatile system that delivers precision at low cost. Permanent magnets are readily available in different shapes, sizes, and strength. Surgical tools or medical devices can be equipped with an appropriate magnet that demands only minimal design changes. Permanent magnets also do not require power, which further reduces the need for the redesign and adaptation of the tool or device to be tracked.

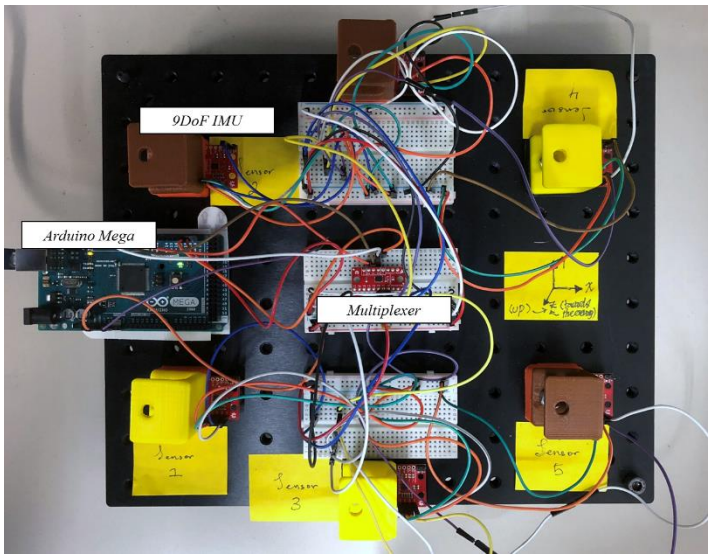

*Figure 1: Sensor Array. Six (6) LSM9DS1 IMU sensors were connected to an Arduino Mega 2560 via I2C. The communication was mediated through a 74HC4051 *-channel multiplexer. The array was fixed to a 300 mm x 300 mm aluminum optics breadboard. Sensors were held in place via 3D-printed standoffs which, in turn, support a secondary aluminum breadboard used as the base of the tracking volume (not shown).*

We picked a 30 mm annular disk permanent magnet for our project. The magnet's dipole field is assumed to be ideal and its dipole moment calculated empirically.

Empirical Approximation of K for Arbitrary Magnet

We devised an empirical approach to approximate the value of K using a single *SparkFun LSM9DS1 IMU* and a custom CNC machine. The CNC was used to move a fitted permanent magnet precisely along the x axis, thus simplifying Eqns. (2), (3) and (4) into Equation (5).

$$\mathrm{K} = \left\|\vec{\mathbf{H}}\right\|^2 x^2 \tag{5}$$

The procedure employed for the approximation of K, for each magnet, can be summarized in the following six steps:

1. The magnet is placed at 50mm away from the IMU sensor such that it reads $H_y, H_z \cong 0$.
2. A sample value for $\left\|\overrightarrow{\mathbf{H}_i}\right\|$ **is** obtained and an accurate approximation for K was computed using Eqn. (5).
3. The magnet is moved by 10 mm in the x-axis.
4. Another sample of K is approximated from a new sample of $\left\|\overrightarrow{\mathbf{H}_i}\right\|$.
5. Steps 3 and 4 are repeated up to x=75mm, recording the values of x, $\left\|\overrightarrow{\mathbf{H}_i}\right\|$ and K each time.
6. An approximated result of K is generated from averaging the sampled points.

The calculated value of K varies along the different x positions. The rigorous characterization of these variations and their impact on the system is left as future work. It is possible to continuously improve the accuracy of the approximated value of K for a magnet by minimizing the H_y and H_z components of the magnetic field during the procedure.

Sensor Array and Tracking Algorithm

To determine the position of the permanent magnet in 3D space, at least three magnetic field measurements are needed. Three independent sensors are required to triangulate the position of the permanent magnet. To enhance the range and accuracy of the tracking system however, an array of six *SparkFun LSM9DS1 IMU* sensors was developed. Due to I^2C address conflicts, magnetometer communication was mediated using a *SparkFun 74HC4051 8-channel multiplexer*. Data was driven through an Arduino-compatible microcontroller such as the *Arduino Mega 2560* or *PJRC's Teensy 3.2* (Figure 1). Microcontrollers formatted and transmitted magnetometer data through a Serial Bus to a PC running a custom Python script. The entire set-up is mounted between two aluminum breadboards with M6 taps every 25 mm. 3D-printed holders were fabricated to secure the magnetometers and permanent magnets.

Sensor readings were taken by the magnetometers at 80Hz, yielding the x, y and z components of $\vec{\mathbf{H}}$ with respect to the sensor orientation. Geomagnetism is partially accounted for using the board's built-in declination adjustment function. To mitigate the effect of ambient magnetic fields, sensor readings are averaged over 50 samples. The resultant, treated as an offset, is then subtracted from later readings. Readings range between ±20 Milligauss and ±16 Gauss, in accordance to the built-in 16-bit analog to digital converter in the chip.

Data retrieval and position tracking was driven by a custom Python script developed on a PC. Based on Eqns. (2), (3) and (4), each magnetometer allows the Python script to assemble one equation, for a total of six equations using the entire array. The resulting non-linear system is solved numerically. SciPy's implementation of the Levenberg-Marquardt (LMA) method is used to solve the resulting non-linear system. The script constructs a determinable system of equations using the data from the three magnetometers observing the largest $\left\|\vec{\mathbf{H}}\right\|$. LMA was chosen for its robustness and speed of convergence. Solutions typically converged within 2 milliseconds. SciPy's LMA combines Newton-Raphson's algorithm and the Steepest Descent method to converge even in the case of a poor initial guess. However, like any numerical method, effective convergence relies on the initial approximation to the solution. To overcome this issue, the centroid of the triangle described by the three magnetometers with the largest readings is used as the initial guess. Upon convergence of the LMA, values are logged to determine point accuracy (Table 1, 2) and motion tracking capabilities (Figure 2).

RESULTS

Approximation of K

Following the CNC-based approximation protocol described earlier, the magnitude of the magnetic field moment for the 30 mm permanent magnet was found to be $K = 1.092 * 10^{-06}\ G^2 m^6$.

Position Tracking Accuracy

Position tracking accuracy was studied by placing the permanent magnet at 18 different locations over the sensor array, varying x, y and z coordinates using 3D-printed standoffs. At each location, sensor readings and position calculations were recorded over 20 seconds. Accuracy was defined as the difference between the expected and observed x, y and z coordinates (Δx, Δy, Δz). The test revealed mean differences of Δx = 1.01 mm, Δy = -0.23 mm and Δz = 2.44 mm, with some significant deviations and variance. All results were consolidated in Table 1. To further asses point accuracy of the system, percent error was calculated by dividing accuracy by the length of magnet's position vector. Errors were found to be Ex = 1.79%, Ey = 1.49% and Ez = 1.97%. The remainder of the statistical data was consolidated within Table 2.

Table 1: Point Accuracy

Statistics	Δx (mm)	Δy (mm)	Δz (mm)
Mean	1.014986704	-0.235216163	2.436613348
Standard Error	0.89239704	0.652383942	0.751564213
Median	0.44202189	0.064654689	2.104299463
Standard Deviation	3.786119992	2.767830657	3.188616911
Sample Variance	14.33470459	7.660886545	10.1672778
Range	14.62381726	10.86607156	14.28932934
Minimum	-3.814912391	-6.182319642	-5.657180441
Maximum	10.80890487	4.683751918	8.632148896
Sum	18.26976067	-4.233890927	43.85904027
Count	18	18	18
Confidence Level(95.0%)	1.882793177	1.376409804	1.585661885

Table 2: Percent Error

Statistics	x/|v| (%)	y/|v| (%)	z/|v| (%)
Mean	1.788990524	1.487774525	1.967210401
Standard Error	0.464697812	0.317758572	0.417654267
Median	1.079502398	0.827137679	1.453988431
Standard Deviation	1.971545846	1.348135446	1.771956984
Sample Variance	3.886993021	1.81746918	3.139831554
Range	6.790801587	4.981248323	6.473280266
Minimum	0.182685395	0.099124798	0.182226135
Maximum	6.973486983	5.080373121	6.655506401
Sum	32.20182943	26.77994144	35.40978722
Count	18	18	18
Confidence Level(95.0%)	0.980426683	0.670411985	0.881173478

Motion Tracking

In addition to static position accuracy, the system was tested for motion tracking. A 3D-printed track was designed to guide the permanent magnet on a constrained path as its position was approximated by the sensor array. Position in 3D space (x, y, and z coordinates of the magnet) was time-stamped and recorded by the sensor array. Scatter plots were generated for each run (Figure 2). To maintain the magnet on the track, a carriage was 3D-printed to hold the magnet. The carriage, in turn, generated a constant offset in the z coordinate of the magnet (Figure 2).

The motion tracking performance of the system was determined by estimating a sampling rate. For eight trials, position measurements were recorded for the duration of one lap around the track. The number of measurements recorded was divided by the lap time to estimate a sampling rate of 23.50 ± 0.0404 samples/sec (N=8).

INTERPRETATION AND FUTURE WORK

The most significant accomplishments of the work presented encompass the design and implementation of a non-contact, position tracking method and system using affordable, open-source hardware and software components. The system provides accurate position results (Δx = 1.01 mm, Δy = -0.23 mm, Δz = 2.44 mm, E_x = 1.79%, E_y = 1.49% and E_z = 1.97% for N=18) and performs over a wider range than other similar applications [2, 5, and 6]. The system also sustained a constant sampling rate of 23.50 ± 0.0404 samples/sec (N=8). This method

works with off-the-shelf permanent magnets, providing easy adaptation to devices or applications.

Throughout the development of our system, our team encountered some limitations which had an effect on the results presented. First, the system and methodology must be refined to account for rotations of the permanent magnet. This may require the integration of rotation calculations as described by Chen *et al.* [5]. Second, the full 3D tracking range of the sensor array must be studied thoroughly. Initial results in 2D and 3D tracking revealed areas and volumes where position accuracy is inconsistent with the results presented here. Understanding range limitations may require automated, accurate testing equipment. CNC systems can be programmed to pursue a path and, therefore, perform an extensive position accuracy test and identify range limits. The same level of automation can be used to more objectively determine the system's performance during motion tracking.

Future work will focus on improving data collection and position calculation algorithms. Continued development will include automated mechanisms to evaluate system performance and hardware improvements to reduce system footprint by implementing micro-computers like the *Raspberry Pi 3*.

REFERENCES

[1] Han, X., Seki, H., Kamiya, Y., and Hikizu, M. "Wearable handwriting input device using magnetic field Geomagnetism cancellation in position calculation." *Precision Engineering* Vol. 33 Issue 1 (2009), pp: 37-43. DOI 10.1016/j.precisioneng.2008.03.008.

[2] Han, X., Seki, H., Kamiya, Y., and Hikizu, M. "Wearable handwriting input device using magnetic field 2nd report: Influence of misalignment of magnet and writing plane." *Precision Engineering* Vol. 34 Issue 3 (2010), pp: 425-430. DOI 10.1016/j.precisioneng.2009.12.005

[3] Raab, F., Blood, E., Steiner, T., and Jones, H. "Magnetic Position and Orientation Tracking System" *IEEE Transactions on Aerospace and Electronic Systems* Vol. AES-15 No. 5 (1979), pp: 709-718

[4] Moeslund, T., and Granum, E. "A Survey of Computer Vision-Based Human Motion Capture." *Computer Vision and Image Understanding* Vol. 81, Issue 3 (2001), pp: 231-268. DOI 10.1006/cviu.2000.0897

[5] Chen, K., Lyons, K., White, S., and Patel, S. "uTrack: 3D Input Using Two Magnetic Sensors" In *Proceedings of the 26th Annual ACM Symposium on User Interface Software and Technology (UIST 2013).* pp: 237-244. St. Andrews, UK, October 8th-11th, 2013. DOI 10.1145/2501988.2502035

[6] Chen, K., Patel, S., and Keller, S. "Finexus: Tracking Precise Motions of Multiple Fingertips Using Magnetic Sensing" In *Proceedings of the 2016 CHI Conference on Human Factors in Computing Systems (CHI 2016), ACM.* pp: 1504-1514. San Jose, California, USA, May 7th-12th, 2016. DOI 10.1145/2858036.2858125

[7] Yoon, S., Huo, K., and Ramani, K. "TMotion: Embedded 3D Mobile Input using Magnetic Sensing Technique" In *Proceedings of the Tenth International Conference on Tangible, Embedded, and Embodied Interaction (TEI 2016), ACM.* pp: 21-29. Eindhoven, Netherlands, February 14th-17th, 2016. DOI 10.1145/2839462.2839463

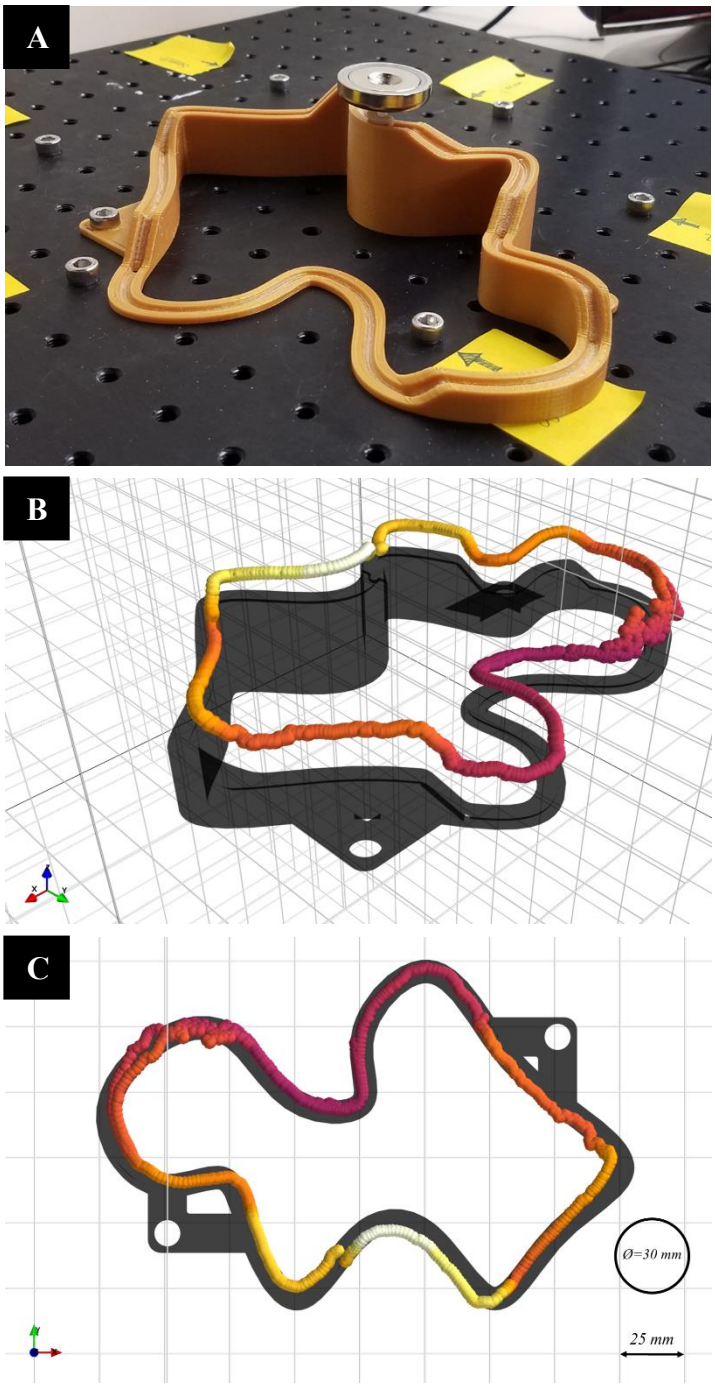

Figure 2: Motion Tracking. (A) 3D-printed track with permanent magnet. (B) Tracking results for a single trial in isometric projection. (C) Top-view of the same results. A color gradient depicts z-position of the magnet. Grid dimensions and reference size of the magnet were included for reference.

[8] Beasley, R. A.: “Medical Robots: Current Systems and Research Directions” In *Hindawi Journal of Robotics Volume 2012, Article ID 401613*. DOI 10.1155/2012/401613

[9] Q. H. Li, L. Zamorano, A. Pandya, R. Perez, J. Gong, and F. Diaz, “The application accuracy of the NeuroMate robot— a quantitative comparison with frameless and frame-based surgical localization systems,” *Computer Aided Surgery, vol. 7, no. 2, pp. 90–98, 2002.*

[10] M. Remacle, V. M. N. Prasad, G. Lawson, L. Plisson, V. Bachy, and S. Van der Vorst, “Transoral robotic surgery (TORS) with the Medrobotics Flex™ System: first surgical application on humans,” *European Archives of Otorhinolaryngology, February, 2015*. DOI 10.1007/s00405-015-3532-x

[11] The Economist, “New surgical robots are about to enter the operating theater,” *The Economist; Science and technology, November 16, 2017.* URL: https://www.economist.com/news/science-and-technology/21731378-surgeons-will-soon-have-more-helping-mechanical-hands-new-surgical-robots-are